Geophysical Research Letters

RESEARCH LETTER
10.1029/2022GL099257

**Key Points:**

- We applied an improved receiver-function method in central midcontinent of the U.S. to construct a refined Moho-depth map
- Our results indicate Moho depth variations of different wavelengths, some of which correspond with known geological structures
- Moho depth variations cross Precambrian boundaries, suggesting a likely post-accretion tectonic modification of the lithosphere

**Supporting Information:**

Supporting Information may be found in the online version of this article.

**Correspondence to:**

X. Song,
xiao.d.song@gmail.com

**Citation:**

Xiao, H., DeLucia, M., Song, X., Li, J., & Marshak, S. (2022). Crustal thickness variations in the central midcontinent, USA, and their tectonic implications: New constraints obtained using the H-κ-c method. *Geophysical Research Letters*, *49*, e2022GL099257. https://doi.org/10.1029/2022GL099257

Received 10 JUN 2022
Accepted 19 AUG 2022



# Crustal Thickness Variations in the Central Midcontinent, USA, and Their Tectonic Implications: New Constraints Obtained Using the H-κ-c Method

**Hongyu Xiao[1], Michael DeLucia[1], Xiaodong Song[1,2], Jiangtao Li[3], and Stephen Marshak[1]**

[1]Department of Geology, University of Illinois at Urbana-Champaign, Urbana, IL, USA, [2]School of Earth and Space Sciences, Institute of Theoretical and Applied Geophysics, Peking University, Beijing, China, [3]Department of Geophysics, School of Geodesy and Geomatics, Wuhan University, Wuhan, China

**Abstract** The central midcontinent of the USA's cratonic platform is a region of low elevation and relief underlain by tectonic basins, domes, faults, and monoclines. To investigate potential correlations among shallow crustal structure and crustal thickness, we produced a high-resolution Moho-depth map of the region by applying the recently developed H-κ-c receiver-function method to data from EarthScope Transportable-Array and Flexible-Array stations. Results indicate that Moho depth varies from 38 to 57 km. Changes of Moho depth and of *Vp*/*Vs* ratios do not correlate with Precambrian tectonic boundaries, suggesting that they reflect post-accretion tectonics. Deeper Moho underlies sedimentary basins, implying a relationship between crustal thickness and lithospheric subsidence. Thicker crust may be due to rift-related underplating, and thinner crust may have undergone delamination. Some depth changes underlie known faults and fold zones. Since short-wavelength undulations were detected only under high-density seismic arrays, they may occur more widely but have yet to be resolved.

**Plain Language Summary** Studies of the central midcontinent region of the USA, a portion of North America's relatively stable craton, reveal that both the Moho (the crust/mantle boundary) and the surface of the Great Unconformity (the boundary between crystalline basement and overlying Phanerozoic sedimentary cover) have kilometers of relief, even though land-surface relief in the region is, at most, 0.5 km. To clarify the nature of variations in Moho depth, so as to make it possible to correlate these variations with other geologic features of the shallow continental crust, we applied a new, more robust, method in estimating Moho depth to data from all available EarthScope seismic stations in the region. This effort yielded a new, high-resolution map of Moho depth. Significantly, we found large undulations (ups and downs) of the Moho both at the regional scale and at the local scale. Some of these undulations correlate with the boundaries of regional basins and domes, as defined by the depth to the Great Unconformity, and others correlate with known faults. The development of thickness variations may reflect geologic events, such as addition of new rock to the base of the crust, or removal of lower crust, which happened after the crust first formed.

## 1. Introduction

The central midcontinent region of the United States—including Missouri, Illinois, Indiana, Kentucky, northern parts of Arkansas, and Tennessee—is a relatively stable cratonic-platform domain where Precambrian crust is overlain by a veneer of Phanerozoic sedimentary strata (e.g., Whitmeyer & Karlstrom, 2007). Epeirogenic movements and localized faulting affected the region during the Phanerozoic (e.g., Braile et al., 1982; Marshak, 2022; Marshak & van der Pluijm, 2021; Sbar & Sykes, 1973; Sykes, 1978). Consequently, the region hosts the Ozark dome (OD) and the Illinois Basin (IB), as well as numerous intraplate fault and fold zones. Some of these zones remain seismically active despite their distance from active plate boundaries (Marshak & Paulsen, 1996; Marshak & van der Pluijm, 2021; Merino et al., 2010; Nuttli, 1979; Petersen et al., 2020; Stein et al., 2012; Sykes, 1978; Williams et al., 2011; Yang et al., 2014). Are these upper-crustal tectonic features related to variations in crustal thickness, as defined by depth to the Moho? To address this question, we have re-analyzed EarthScope data from seismic arrays in the Midcontinent, using a refined method to analyze receiver-function (RF) data.

RF techniques, in general, can determine the depth to a seismic discontinuity in the Earth by analyzing the travel time difference between P-waves and S-waves, generated by the P-to-S conversion of teleseismic waves crossing the discontinuity, as recorded by a three-component seismograph at a receiving station (Langston, 1977).

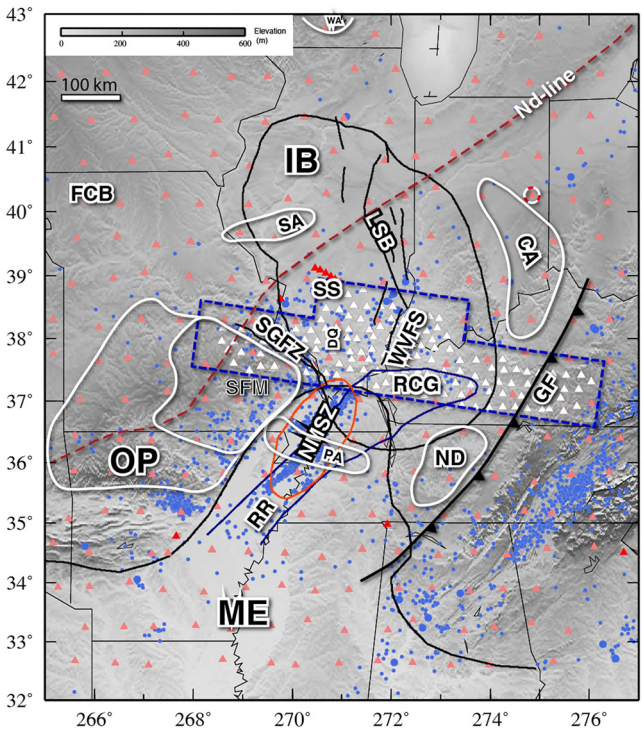


**Figure 1.** Station distribution, simplified major geological structures, and historical seismicity in the central midcontinent. Stations are marked by triangles: Transportable array stations are pink, and the OIINK flexible rray stations are white. Other stations are red. The white/red dashed circle marks the location of the example station in Figure 2. The dashed blue line delimits the densely covered area. The maroon dashed line delimits the Nd-line. The solid red line delimits the New Madrid Seismic Zone area. Blue dots are historically seismicity. The areas enclosed by white lines indicate domes and arches. Abbreviations: WA, Wisconsin Arch; IB, Illinois Basin; FCB, Forest City Basin; SA, Sangamon Arch; LSB, LaSalle Belt; CA, Cincinnati Arch; FA, Findlay Arch; SGFZ, Ste. Genevieve Fault Zone; SS, Sparta Shelf; DQ, DeQuoin Monocline; WVFS, Wabash Valley Fault System; RCG, Rough Creek Graben; SFM, St. Francois Mts., the apex of the Ozark Dome; NMSZ, New Madrid Seismic Zone; OP, Ozark Plateau; PA, Pascola Arch; RR, Reelfoot Rift; ND, Nashville Dome; GF, Grenville Front; and ME, Mississippi Embayment.

Modeling the RFs (amplitudes and timings of the converted waves) captured by many stations over a region provides valuable constraints on the depth to the Moho, the profound seismic discontinuity between crust and mantle, and therefore on crustal thickness. For example, by stacking the RFs at different azimuths and distances, H (crustal thickness), and κ (*Vp*/Vs ratio) can be estimated by using the H-κ method (Zhu & Kanamori, 2000). In the present study, we utilized a recent modification of the H-κ method. This modification, called the H-κ-c method (Li et al., 2019) adds a harmonic correction ('c') to the H-κ method, and therefore, can provide a more accurate and stable Moho depth estimation than came from previous studies. In the H-κ-c method, trigonometric fitting is applied to make harmonic corrections to Moho P to S converted phases and their crustal multiples, thereby reducing the influence of a tilted Moho and of crustal anisotropy on results. These correction result in improved estimates of H and κ.

The H-κ-c method is particularly useful in areas with complicated crustal structure and variable Moho depth. It can yield results that differ significantly from those using other techniques. In fact, studies of crustal structure in China show that Moho depth calculated from the H-κ-c method can be as much as 5 km different from those determined using the traditional H-κ method, and the κ estimate difference could be as large as 0.09 (Li and Song, 2021; Li et al., 2019).

Given previous evidence for large vertical relief of the Moho over short horizontal distance in the Midcontinent (Yang et al., 2017), the region's Moho surface likely would be tilted significantly in many locations, so a traditional receiver function study, that assumes a relatively flat Moho and isotropic crust, would introduce bias into the estimates of the Moho depth. Fortunately, regional seismic-array experiments have been deployed within the central Midcontinent during the last decade (Figure 1), allowing a higher-resolution crustal thickness map of the region that permits investigation of links between thickness variations and upper-crustal features. The combination of the station coverage and the new H-κ-c method allows us to construct a new high-resolution crustal thickness map of the central midcontinent. With the updated map, we could investigate possible links between Moho depth variations and upper-crustal and surficial geologic features.

The seismic arrays we used include the Wabash Valley Seismic Zone network (6E), Cooperative New Madrid Seismic Network (NM), The Florida to Edmonton Broadband Experiment (XR), Earthscope Transportable Array (TA), and the OIINK (for Ozarks, Illinois, Indiana, and Northern Kentucky) Flexible Array (FA). The OIINK FA was an experiment that augmented TA stations, so that station density was improved from about 70 km between stations to approximately 25 km between stations (Hamburger et al., 2012). This array spanned several major geological features including the OD, IB, the Rough Creek Graben (RCG), and the Grenville front (GF), as well as several seismically active fault zones, including the Ste. Genevieve fault zone (SGFZ), the Wabash Valley fault zone (WVFZ), and the northern extension of the New Madrid seismic zone (NMSZ). Other abbreviations used in the paper, are identified in Figure 1.

Below, after briefly summarizing the geologic context of our study area, we describe our analytical method. Then, we present our new crustal-thickness map, and compare it to that of a previous study. We conclude by discussing potential relationships between depth-to-Moho variations and known tectonic and stratigraphic features of the upper crust and land-surface.

## 2. Geological Background

The central Midcontinent region is a particularly interesting region of North America's cratonic platform, for it contains notable intracratonic seismic belts, pronounced epeirogenic structures (basins, domes, and arches), belts of documented faulting and associated monoclinal folding, and boundaries delineating Precambrian tectonic provinces. Therefore, this region hosts numerous intracratonic tectonic features with which variations in Moho depth can be compared.

Crust of the central Midcontinent assembled during the Proterozoic when NE-trending accretionary orogens, including the Yavapai Province and the Mazatzal Province, accreted to Archean and Paleoproterozoic crustal provinces (Whitmeyer & Karlstrom, 2007). The 1.47 Ga Eastern Granite-Rhyolite (EGR) province overprints these terranes and includes the enigmatic "Nd-line" which defines the eastern limit of Geon 16 juvenile crustal ages (Bickford et al., 2015; Chen et al., 2018; Van Schmus et al., 1996). A recently recognized tectonic province—the Picuris-Baraboo orogen, of similar age to the Granite-Rhyolite province—may also lie within the region (Medaris et al., 2021). The Grenville Front (GF) marks the eastern limit of ∼1.1 Ga deformation and metamorphism in the region.

Subsequent to the assembly and cratonization of the Midcontinent region, epeirogenic displacements produced distinct cratonic-interior basins, arches, and domes (e.g., Marshak & van der Pluijm, 2021). The study area includes the IB, which covers parts of Illinois, Indiana, western Kentucky, Tennessee, and eastern Missouri, and contains sequences of Paleozoic sedimentary strata (Bedle & van der lee, 2006; Klein, 1995; Kolata & Nelson, 1990; McBride & Kolata, 1999; McBride et al., 2003). The land surface of the basin presently lies at an elevation of about 200 m. Its base, as defined by the position of the Great Unconformity (the boundary between Paleozoic strata and underlying 1.47 Ga basement), reaches a maximum depth of about 7 km (e.g., Bedle & van der lee, 2006). The IB lies to the east of the OD. Within the OD, Paleozoic strata thin and Precambrian basement has been exposed. Presently, the apex of this structural dome underlies a topographic high, the St. Francois Mts. at the northeast corner of the Ozark Plateau. Here, the land surface reaches an elevation of 540 m. The Great Unconformity, consequently, displays a maximum structural relief of about 7.5 km within our study area (Marshak et al., 2017). The region also contains several distinct midcontinent fold and fault belts, such as the LaSalle Belt of Illinois, in which Phanerozoic reactivation of Proterozoic faults produced monoclinal folds (e.g., Marshak & Paulsen, 1996, 1997).

Presently, the central midcontinent area hosts three notable seismic zones. The most active of these is the NNE-trending NMSZ, which underlies the northern Mississippi Embayment (ME)—its activity represents reactivation of faults within the Reelfoot Rift (RR) (Nelson et al., 1985; Williams et al., 2011; Zhan et al., 2017). The SGFZ involves a NW-trending fault system located near the boundary between Illinois and Missouri (Nelson et al., 1985; Yang et al., 2014). The WVFZ is a seismically active area that trends NNE-SSW, along the southern portion of the Illinois-Indiana border (Obermeier et al., 1991). Historically, more than 30 earthquakes with a magnitude greater than 5, as well as the thousands of smaller seismic events, have occurred in central midcontinent (Nuttli, 1979; Pavlis et al., 2002).

Recently, Yang et al. (2017) showed that the depth to the Moho varies significantly over short horizontal distances in the central Midcontinent. They state that crust increases in thickness from 45 km below the OD to more than 60 km beneath the Sparta Shelf (the western portion of the IB). This vertical relief of >15 km occurs over a horizontal distance of less than 100 km. The boundary between these two regions approximately underlies the SGFZ, which lies within the transition from the OD into the IB (Figure 1; Marshak et al., 2017; Yang et al., 2017), so a possible correlation has been suggested between relief of the Great Unconformity and crustal-thickness variations (DeLucia et al., 2019; Marshak et al., 2017; Stein et al., 2018; Yang et al., 2017).

## 3. Data and Methods

In this study, we used the H-κ-c method (Li et al., 2019), which corrects for dipping interfaces and anisotropy, by applying harmonic functions, before stacking Ps and their crustal multiples in the receiver functions. We collected data from a total of 333 broad-band seismic stations in the central Midcontinent for a 5.5-year-long time period extending from October 2010 to April 2016. The stations were from the following networks: 181 from EarthScope's TA, 143 from the OIINK FA experiment (XO), 5 from Wabash Valley Seismic Zone network (6E),

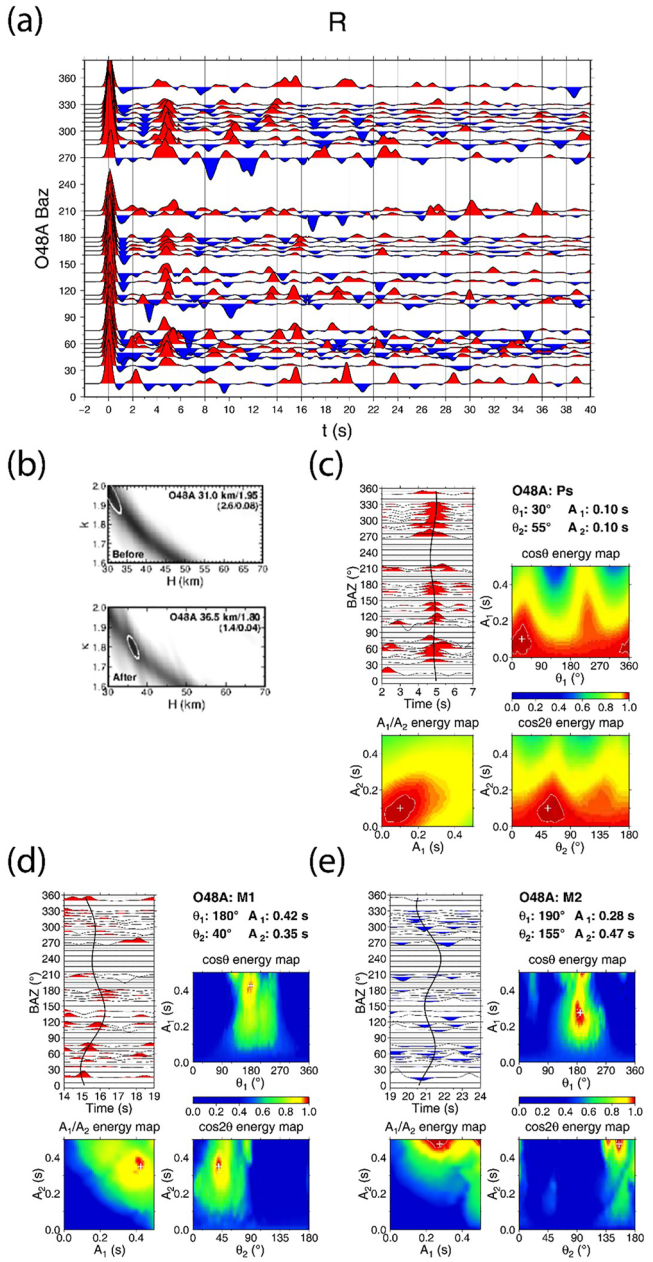


**Figure 2.** An example of H-κ-c correction results for a Station O48A. (a) Record section of receiver functions, sorted by azimuth, after H-κ-c (grouped every 5°). (b) A comparison between the traditional H-κ (top) stacking and H-κ-c stacking (bottom) using the same data, H representing crustal thickness and κ representing *Vp*/*Vs* ratio. From Li et al. (2019), cos$\theta$ and cos2$\theta$ functions were used to fit the arrival times of Ps and crustal multiples with BAZ ($\theta$) by $F(\theta) = A_0 + A_1\cos(\theta - \theta_1) + A_2\cos2(\theta - \theta_2)$, where $A_0$ is the central arrival time and $A_1$, $A_2$, and $\theta_1$, $\theta_2$ are the amplitudes and phases of the two-lobed and four-lobed variations. (c) Record section of the Ps phase used in the H-κ-c correction, and the best fit trigonometric solution. (d) Record section of the M1 (PpPs) phase used in H-κ-c correction, and the best-fit trigonometric solution. (e) Record section of the M2 (PpSs + PsPs) phase used in H-κ-c correction and the best-fit trigonometric solution.

3 from Cooperative New Madrid Seismic Network (NM), and 1 from The Florida to Edmonton Broadband Experiment (XR) (Figure 1). The duration of the data collection at each station varies from 14 months to over 5 years. For RF calculations, we selected a total of 5,159 teleseismic events that had a magnitude of 5 or greater and lay at a distance of between 30° and 95° from the study area (Figure S1 in Supporting Information S1). For the application of the H-κ-c method, we used only stations with at least two years of events, which helps prevent the azimuthal coverage gap from exceeding 90° and ensure stable solutions for the harmonic corrections (Li et al., 2019).

We retrieved 3-component time series data from IRIS data center. Each waveform was cut from 50 s before the first P arrival to 150 s after the first P arrival. Before processing, we used a bandpass filter with 0.05–2 Hz frequency range on all waveforms. We then resampled all the waveform data to the same sample rate of 10 samples per second and rotated from the ZNE system to the RTZ system. We then followed the four major processing procedures in Li et al. (2019). First, we applied the traditional H-κ stacking method and procured the reference arrival times of Ps and the crustal multiples. Second, we performed the moveout correction with epicentral distance. Third, we used trigonometric functions (cos$\theta$ and cos2$\theta$ functions, $\theta$ is the back azimuth) to fit the back azimuthal variations of Ps and their crustal multiples (M1 and M2, which stands for PpPs and PpSs + PsPs, respectively). Finally, we corrected the receiver functions on Ps and multiples (correct every phase to corresponding central arrival time) and performed the H-κ stacking with the corrected receiver functions and obtained the final estimates. For processing details, please refer to Li et al. (2019). Notably, the H-κ-c method requires at least 1 receiver function per 90° to ensure the robustness of the harmonic correction solutions.

## 4. Results

The H-κ-c method described above provides a better estimate of Moho depth, and results in less uncertainty, than does the traditional H-κ method (Figure 2; Figure S2 in Supporting Information S1). Figure 2 illustrates this improvement for Station O48A. For this station, results from the H-κ-c method and from the traditional H-κ method differ by 5.5 km in H, and 0.15 in κ. The H-κ-c method also reduces the error for H from 2.6 to 1.4 km, and reduces error for κ from 0.08 to 0.04 (Figure 2b). The Ps phase (Figure 2c) and its crustal multiple (Figure 2d) are better aligned by the harmonic fittings, and the stacking energy is better focused after the H-κ-c method corrections are made (Figure 2b). Given the 2 years worth of data availability, the existence of an RF trace for every 90° azimuth, the reduction of estimation error, and the trigonometric correction, our method produces consistent and robust solutions for Ps, and often for M1 and M2 as well for most stations (e.g., Figure 2 and Figure S3 in Supporting Information S1).

Results using the H-κ-c method display improved accuracy (i.e., produced smaller error ellipses) for both crustal-thickness and *Vp*/*Vs* ratio estimates, than could be obtained by the traditional H-κ method, for 262 out of the total 333 stations (Figure S2 and Table S1 in Supporting Information S1). The rest of the stations (71) that did not show improvement were ones for which azimuth coverage was poor, or data quality was low. The distributions of the determined crustal thickness and *Vp*/*Vs* ratios and their error estimates, are shown in Figure S5 and Table S1 in Supporting Information S1. The average

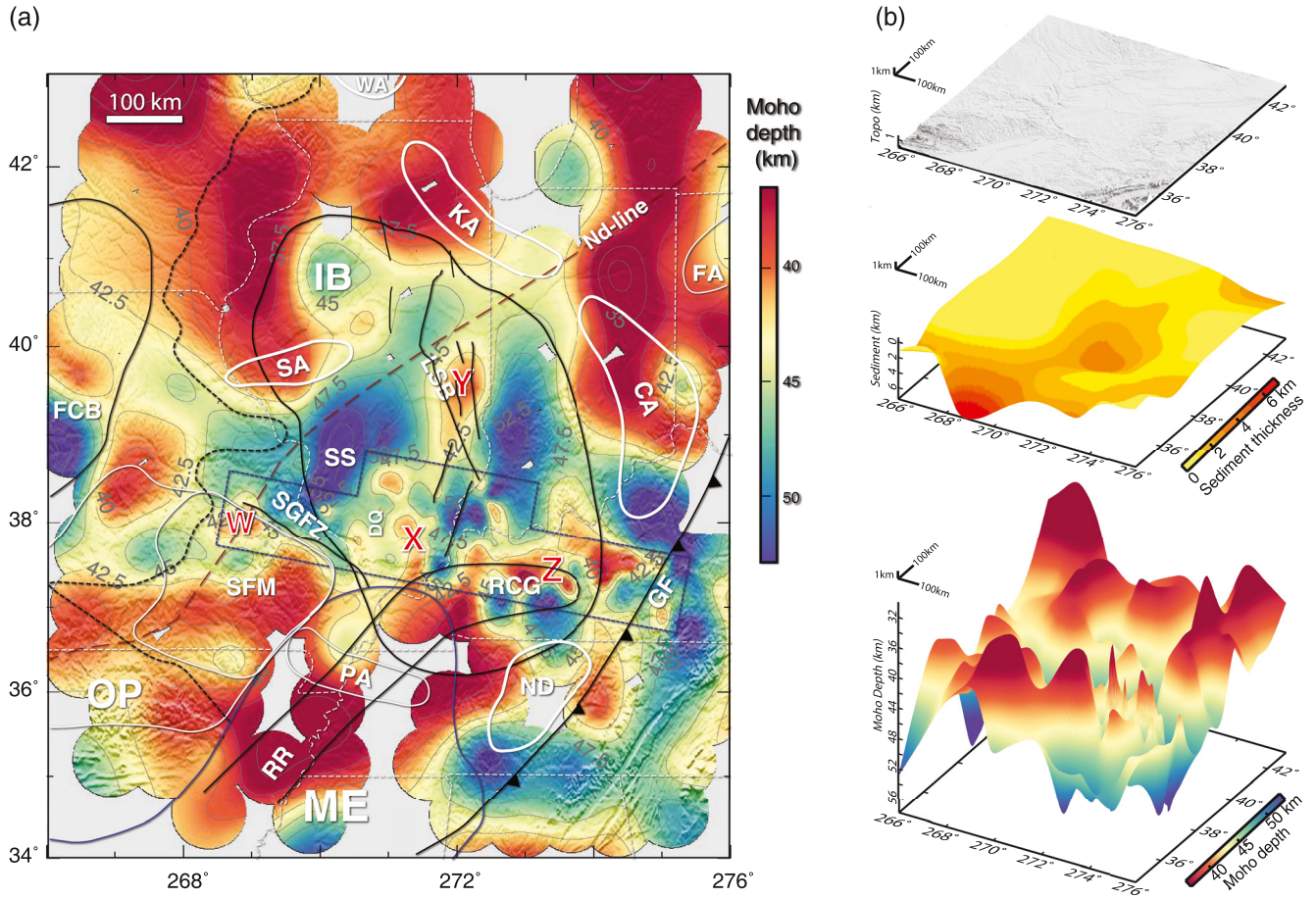


**Figure 3.** Results of crustal thickness obtained in this study. (a) A Moho depth map in the central midcontinent of US from the H-κ-c method. Stations with good quality were plotted with a 50 km radius of influence while stations with poor results were grayed out. Relief difference between adjacent contour line is 2.5 km. (b) A 3-D view of surface topography, sedimentary basement, and Moho topography (from top to bottom). Vertical and horizontal scales were marked at the upper left corners. See Figure 1 for the scale of surface topography. Abbreviations and lines delineating different regions are the same as in Figure 1. The black dashed line = EGR boundary; the maroon dashed line = the Nd-line.

uncertainty (standard deviation) is 2.1 km for crustal thickness (H) and 0.05 for *Vp*/*Vs* ratio. We used only the stations with improved H-κ-c results for further analysis.

Figure 3 displays the results of crustal thickness from the H-κ-c method, as constructed using the 262 stations with improved accuracy. Each station represents a 50 km radius of influence, which is approximately the horizontal range of the crustal multiples at the Moho depth. Results of different stations are gridded using the "surface" algorithm in GMT (Wessel & Smith, 1998). Comparison of our results to those of Yang et al. (2017) shows similar regional patterns. But our new map displays greater resolution and thus highlights smaller-scale structures and local slopes in the Moho more clearly.

Overall, our results indicate that crustal thickness under the study area ranges from 38 to 57 km, with an average of 44 km. This range resembles that produced by the continental US crustal-thickness model of Shen and Ritzwoller (2016), but is less than the estimate of Yang et al. (2017). The region of increased crustal thickness, where crust reaches a thickness of about 52–57 km, occurs underneath the Sparta Shelf, the relatively shallow western portion of the IB. Our analysis indicates that the region of very thick crust covers a larger area than that shown on Yang et al. (2017) map. Notably, the area of thicker crust is clearly bounded by known crustal structures (the Sangamon Arch to the north, the La Salle Belt to the east, and the SGFZ to the southwest). The LaSalle Belt is more distinct on our Moho-depth map than to the findings on Yang et al. (2017) map. In fact, our map suggests that a relatively narrow, segmented belt of relatively thinner crust underlies the LaSalle Belt and the DuQuoin Monocline. This belt may link at its southern end to the junction of the RR and the RCG. The greatest depth of the

Moho (57 km) beneath the Sparta Shelf area occurs beneath Station Q43A, and is about 10 km shallower than the estimate of Yang et al. (2017). Of note, the RFs for this station are complex, and display weak crustal multiples, making it difficult to determine the H and κ values (Figure S3 in Supporting Information S1). Since the H-κ-c method helps reduce the effect of crustal complexities and focuses stacked energy better, we infer that this method yields a better estimate of H and κ than does the conventional H-κ method alone.

Our results reveal Moho undulations (crustal-thickness variations) of more than one apparent length scales in the central Midcontinent (Figure 3a). In the following, we define wavelength as the horizontal distance between adjacent Moho-depth minimums or between adjacent Moho-depth maximums. Notably, the shorter wavelength features occur primarily within the OIINK array area, suggesting that variations in Moho depth may simply reflect station density. Specifically, within the OIINK array area where stations are densely distributed, crustal thickness varies between 36 and 50 km over a horizontal distance of 60 km. In contrast, in the northern part of the IB, which hosts only TA stations distributed 70 km from each other, similar variations in Moho depth appear to occur over a horizontal distance of 180–200 km. Long-wavelength (wavelength of about 1°) Moho depth variations occur outside of the OIINK array area. Also, we found the maximum Moho depth difference is 18 km in OIINK array area, while the maximum Moho depth difference in the north part of the IB is approximately 9 km. Notably, κ values display a wavelength similar to that of crustal thickness and are generally large (ranging from 1.73 to over 1.90, Figure S4 and Table S1 in Supporting Information S1), more like those (1.73–1.80) obtained also from the improved H-κ-c method for an active tectonic region such as the Tibetan Plateau (Chen et al., 2021; Li et al., 2019; Li & Song, 2021) rather than those (1.65–1.75) for a stable block such as the South China (Cathaysia block) (Deng et al., 2019; Li et al., 2019).

## 5. Discussion

Our refined Moho-depth map of the central Midcontinent in the USA confirms Yang et al. (2017) proposal that Moho depths vary significantly beneath the cratonic platform and can locally reach thicknesses much greater than average values. Our results also confirm that the Moho depth increases abruptly across the boundary between the (OD, marked as SFM on the figures, the apex of the OD) and the western IB, in the region bordering the St. Francois Mts. This prominent discontinuity in Moho depth approximately follows both the SGFZ (Figure 3a), and a major step in the Great Unconformity (e.g., Marshak et al., 2017). The deepest Moho occurs about 55 km east of St. Louis, in southwestern Illinois (Figure 3a). Notably, our results hint that Moho depth undulates at two length scales. Long-wavelength undulations are elongate and have a wavelength of about 1°. Short-wavelength undulations have a wavelength of about 0.5° and are circular to elliptical in map view. Below, we present hypotheses to explain the existence of both types of undulations.

As illustrated in Figure 3a, long-wavelength undulations of the study area roughly correspond with first-order epeirogenic structures (i.e., regional-scale basins, domes, and arches) of the cratonic platform. Specifically, the Moho beneath much of the Kankakee Arch, the Cincinnati Arch, the SFM (the apex of OD), the Pascola Arch, and the Nashville Dome generally lies at a depth of between about 45 and 38 km. In contrast, much of the Moho beneath IB lies at depths of between 45 and 57 km (Figure 3a). Therefore, the crust beneath basement highs (areas where the Great Unconformity lies at shallower depths) in the Midcontinent tends to be thinner (by a few to 20 km) than that of basement lows (areas where the Great Unconformity lies at greater depths). Similarly, crust beneath Ozark Plateau of higher elevation is thinner than beneath the IB of lower elevation. This relationship is the opposite of the familiar relationship between crustal thickness and basement elevation and topographic elevation found in Cenozoic orogenic provinces such as the Tibetan Plateau (Bao et al., 2015; Li & Song, 2021; Li et al., 2022).

What geological phenomena could account for the observed thickening or thinning? If intracratonic basins initiated at the beginning of the Phanerozoic due to crustal rifting, the thickening may be due to underplating (McGlannan & Gilbert, 2016; Medaris et al., 2021; Thybo & Artemieva, 2013) and sill intrusion that accompanied or followed the rifting processes (Chen et al., 2016). Such addition of substantial volumes of mafic rock to the base of the crust has been documented beneath the Midcontinent Rift, to the west of our study area (Moidaki et al., 2013; Shen et al., 2013), and their presence may be indicated by the horizontal seismic reflectors exist in deep basement crust beneath the IB (McBride et al., 2016). Furthermore, previous research found prominent thickened crust beneath Wyoming craton as well (Rumpfhuber et al., 2009), which has been interpreted to be

associated with added mafic lower crust contributing to local crustal thickening. Thus, Precambrian rift-related underplating could have thickened the crust beneath the IB with dense rock, leading to the basin's subsidence.

Zones of thinner crust either represent regions where no underplating took place or are areas where eclogitized lower crust delaminated prior to cratonization. Such delamination could be associated with the igneous events that produced the ~1.47 Ga EGR Province (Bickford et al., 2015). Differentiation of so much felsic magma left a silica-depleted lower crust/lithospheric mantle, which could have encouraged separation and delamination of mafic/ultramafic lower crust. This hypothesis is similar to one proposed to explain crustal structure of the Sierra Nevada region (Zandt et al., 2004). The interpretation of thickened crust with denser lower crust and mantle lithosphere beneath the IB and thinner crust with lighter lower crust and mantle lithosphere in the surrounding regions is consistent with the gravity anomalies, which is generally larger in the IB than in the surroundings (Figure S6 in Supporting Information S1).

Our Moho-depth map also suggests that Moho-depth variations are not controlled by Precambrian crustal-province boundaries. For example, there is no consistent correlation of Moho depth change with the Yavapai/Mazatzal boundary, with the Nd-line, or with the boundaries of the EGR Province. Though the crust is generally thicker to the southeast of the GF, Moho-depth variability is evident on either side of the structure (Figure 3). These observations imply that the modification of crustal thickness that caused the observed long-wavelength undulations did not develop during crustal amalgamation. We cannot rule out the hypothesis, however, that the region of thickened crust is a result of a collision event that had crustal blocks of varying thickness along strike, or that it was related to variable thickening during the enigmatic Picuris Orogeny (Medaris et al., 2021).

Because of their correlation with station density, short-wavelength Moho-depth variations may merely reflect the resolution of our data. If so, short-wavelength undulations of the crustal thickness could be more pervasive in cratonic crust than previously recognized. Such a result can be tested if other dense seismic arrays are set up in the Midcontinent. The pervasive distribution of short-wavelength Moho undulations would imply that topography of the Moho is more complex than that of regional land-surface elevation variations. The widespread short-wavelength undulations could be a manifestation of localized underplating or delamination, of Moho mobility at times when heat flow was greater, or of displacements associated with Midcontinent fault-and-fold zones.

The association of some short-wavelength Moho undulations with Midcontinent fault and fold zones is suggested by the proximity of the features and evidence for transcrustal faulting (e.g., DeLucia et al., 2019). For examples, undulations in the vicinity of Point W in Figure 3a appear to align along the SGFZ, those near Point X align with the DuQuoin Monocline, those near Point Y lie within the La Salle Belt, and those near Point Z lie along the RCG. If, as suggested by Marshak and Paulsen (1996), the fault and fold belts represent reactivation of Proterozoic extensional faults, the relatively thin crust observed at these locations today may have developed in Proterozoic rifts that did not undergo underplating. Conceivably, the lack of underplating left these zones weaker, explaining why they continue to be more seismogenic than surrounding areas.

## 6. Conclusions

We produced a refined map of Moho depth variations in the central midcontinent of the United States by using updated station coverage and by analyzing data using the new H-κ-c method. The H-κ-c method corrects for the presence of dipping boundaries and for anisotropy. Comparison of our map with those produced by earlier studies, shows that this method can provide higher-resolution results than could earlier RF methods. Our results show that Moho depth in cratonic platform of our study area varies from 38 to 57 km, and undulates, at two different wavelengths. Long-wavelength variations do not correlate with Precambrian accretionary belt boundaries but do correlate, approximately, with the distribution of regional-scale basins, domes, and arches. Specifically, crust tends to be thicker beneath basins than beneath domes and arches. Short-wavelength variations were recognized primarily in regions beneath high-density seismic arrays. This relationship hints that such features could occur much more broadly than we observed and would have been seen if EarthScope's TA was as dense as the OIINK array. Widespread short-wavelength variations may reflect localized crustal thickening or thinning and greater mobility of the lower crust and mantle during the Mesoproterozoic. Alternatively, some short-wavelength undulations may reflect areas that escaped significant underplating.

## Data Availability Statement

All the seismic data in this study were obtained from the Data Management Center of Incorporated Research Institutions for Seismology at http://ds.iris.edu/wilber3/find_event. In addition, USArray information could be retrieved from https://doi.org/10.7914/SN/TA. The OIINK project data could be found at https://doi.org/10.7914/SN/XO_2011. Network 6E information is available at https://doi.org/10.7914/SN/6E_2013. H-κ-c package could be obtained at https://github.com/ljt-uiuc/H-k-c from Li et al., 2019 (https://doi.org/10.1029/2018JB016356) and is permanently archived at https://doi.org/10.5281/zenodo.7017948. Figures were plotted using GMT (Wessel & Smith, 1998 at https://doi.org/10.1029/98EO00426). The complied H-κ-c results were available at https://doi.org/10.5281/zenodo.5842334.

**Acknowledgments**
We thank insightful and constructive comments from two anonymous reviewers, which helped in improving the manuscript. S. Marshak would like to acknowledge helpful discussions over the years with the OIINK research group. This research was supported by the National Natural Science Foundation of China (Grant No. U1939204) and the U.S. National Science Foundation (EAR 1620595).

## References

Bao, X., Song, X., & Li, J. (2015). High-resolution lithospheric structure beneath mainland China from ambient noise and earthquake surface-wave tomography. *Earth and Planetary Science Letters*, *417*, 132–141. https://doi.org/10.1016/j.epsl.2015.02.024

Bedle, H., & van der Lee, S. (2006). Fossil flat-slab subduction beneath the Illinois Basin, USA. *Tectonophysics*, *424*(1–2), 53–68. https://doi.org/10.1016/j.tecto.2006.06.003

Bickford, M. E., Van Schmus, W. R., Karlstrom, K. E., Mueller, P. A., & Kamenov, G. D. (2015). Mesoproterozoic-trans-Laurentian magmatism: A synthesis of continent-wide age distributions, new SIMS U–Pb ages, zircon saturation temperatures, and Hf and Nd isotopic compositions. *Precambrian Research*, *265*, 286–312. https://doi.org/10.1016/j.precamres.2014.11.024

Braile, L. W., Keller, G. R., Hinze, W. J., & Lidiak, E. G. (1982). An ancient rift complex and its relation to contemporary seismicity in the New Madrid seismic zone. *Tectonics*, *1*(2), 225–237. https://doi.org/10.1029/tc001i002p00225

Chen, C., Gilbert, H., Andronicos, C., Hamburger, M. W., Larson, T., Marshak, S., et al. (2016). Shear velocity structure beneath the central United States: Implications for the origin of the Illinois Basin and intraplate seismicity. *Geochemistry, Geophysics, Geosystems*, *17*(3), 1020–1041. https://doi.org/10.1002/2015gc006206

Chen, C., Gilbert, H., Fischer, K. M., Andronicos, C. L., Pavlis, G. L., Hamburger, M. W., et al. (2018). Lithospheric discontinuities beneath the U.S. Midcontinent—Signatures of proterozoic terrane accretion and failed rifting. *Earth and Planetary Science Letters*, *481*, 223–235. https://doi.org/10.1016/j.epsl.2017.10.033

Chen, L., Wang, W., & Zhang, L. (2021). Crustal thickness in Southeast Tibet based on the SWChinaCVM-1.0 model. *Earthquake Science*, *34*(3), 1–15. https://doi.org/10.29382/eqs-2021-0010

DeLucia, M. S., Murphy, B. S., Marshak, S., & Egbert, G. D. (2019). The Missouri high-conductivity belt, revealed by magnetotelluric imaging: Evidence of a trans-lithospheric shear zone beneath the Ozark Plateau, Midcontinent USA? *Tectonophysics*, *753*, 111–123. https://doi.org/10.1016/j.tecto.2019.01.011

Deng, Y., Li, J., Peng, T., Ma, Q., Song, X., Sun, X., et al. (2019). Lithospheric structure in the Cathaysia block (South China) and its implication for the late mesozoic magmatism. *Physics of the Earth and Planetary Interiors*, *291*, 24–34. https://doi.org/10.1016/j.pepi.2019.04.003

Hamburger, M., Pavlis, G., Gilbert, H., Marshak, S., Larson, T., & Rupp, J. (2012). An Earthscope experiment focuses on North America's continental interior. *EarthScope onSite fall 2012*, incorporated research institutions for seismology.

Klein, G. D. (1995). Intracratonic basins. *Tectonics of sedimentary basins*, 459–478.

Kolata, D. R., & Nelson, W. J. (1990). Tectonic history of the Illinois Basin. *American Association of Petroleum Geologists Memoir*, *51*, 263–285.

Langston, C. A. (1977). The effect of planar dipping structure on source and receiver responses for constant ray parameter. *Bulletin of the Seismological Society of America*, *67*(4), 1029–1050.

Li, J., Song, X., Wang, P., & Zhu, L. (2019). A generalized H-κ method with harmonic corrections on Ps and its crustal multiples in receiver functions. *Journal of Geophysical Research: Solid Earth*, *124*(4), 3782–3801. https://doi.org/10.1029/2018jb016356

Li, J. T., & Song, X. D. (2021). Crustal structure beneath the Hi-CLIMB seismic array in the central-western Tibetan Plateau from the improved H-κ-c method. *Earthquake Science*, *34*(3), 199–210. https://doi.org/10.29382/eqs-2021-0002

Li, M., Song, X., Li, J., & Bao, X. (2022). Crust and upper mantle structure of East Asia from ambient noise and earthquake surface wave tomography. *Earthquake Science*, *35*(2), 71–92. https://doi.org/10.1016/j.eqs.2022.05.004

Marshak, S. (2022). *Earth: Portrait of a planet* (7th ed.). W.W. Norton & Company.

Marshak, S., Domrois, S., Abert, C., Larson, T., Pavlis, G., Hamburger, M., et al. (2017). The basement revealed: Tectonic insight from a digital elevation model of the great unconformity, USA cratonic platform. *Geology*, *45*(5), 391–394. https://doi.org/10.1130/g38875.1

Marshak, S., & Paulsen, T. (1996). Midcontinent US fault and fold zones: A legacy of proterozoic intracratonic extensional tectonism? *Geology*, *24*(2), 151–154. https://doi.org/10.1130/0091-7613(1996)024<0151:musfaf>2.3.co;2

Marshak, S., & Paulsen, T. (1997). Structural style, regional distribution, and seismic implications of midcontinent fault-and-fold zones, United States. *Seismological Research Letters*, *68*(4), 511–520. https://doi.org/10.1785/gssrl.68.4.511

Marshak, S., & van der Pluijm, B. A. (2021). Tectonics of the continental interior in the United States. In D. Alderton & S. A. Elias (Eds.), *Encyclopedia of geology* 2nd ed. (Vol. 4, pp. 173–186).

McBride, J. H., & Kolata, D. R. (1999). Upper crust beneath the central Illinois Basin. *The Geological Society of America Bulletin*, *111*(3), 375–394. https://doi.org/10.1130/0016-7606(1999)111<0375:ucbtci>2.3.co;2

McBride, J. H., Kolata, D. R., & Hildenbrand, T. G. (2003). Geophysical constraints on understanding the origin of the Illinois Basin and its underlying crust. *Tectonophysics*, *363*(1–2), 45–78. https://doi.org/10.1016/s0040-1951(02)00653-4

McBride, J. H., Leetaru, H. E., Keach, R. W., & McBride, E. I. (2016). Fine-scale structure of the precambrian beneath the Illinois Basin. *Geosphere*, *12*(2), 585–606. https://doi.org/10.1130/ges01286.1

McGlannan, A. J., & Gilbert, H. (2016). Crustal signatures of the tectonic development of the North American midcontinent. *Earth and Planetary Science Letters*, *433*, 339–349. https://doi.org/10.1016/j.epsl.2015.10.048

Medaris, L. G., Jr., Singer, B. S., Jicha, B. R., Malone, D. H., Schwartz, J. J., Stewart, E. K., et al. (2021). Early mesoproterozoic evolution of midcontinental Laurentia: Defining the geon 14 Baraboo orogeny. *Geoscience Frontiers*, *12*(5), 101174. https://doi.org/10.1016/j.gsf.2021.101174

Merino, M., Stein, S., Liu, M., & Okal, E. A. (2010). Comparison of seismicity rates in the New Madrid and Wabash Valley seismic zones. *Seismological Research Letters*, *81*(6), 951–954. https://doi.org/10.1785/gssrl.81.6.951

Moidaki, M., Gao, S. S., Liu, K. H., & Atekwana, E. (2013). Crustal thickness and Moho sharpness beneath the Midcontinent rift from receiver functions. *Research in Geophysics*, *3*(1). https://doi.org/10.4081/rg.2013.e1

Nelson, W. J., Lumm, D. K., & Schwalb, H. R. (1985). Ste. Genevieve Fault Zone, Missouri and Illinois. Contract/grant report 1985-03.

Nuttli, O. W. (1979). Seismicity of the central United States. *Reviews in Engineering Geology*, *4*, 67–93.

Obermeier, S. F., Bleuer, N. R., Munson, C. A., Munson, P. J., Martin, W. S., McWilliams, K. M., et al. (1991). Evidence of strong earthquake shaking in the lower Wabash Valley from prehistoric liquefaction features. *Science*, *251*(4997), 1061–1063. https://doi.org/10.1126/science.251.4997.1061

Pavlis, G. L., Rudman, A. J., Pope, B. M., Hamburger, M. W., Bear, G. W., & Al-Shukri, H. (2002). Seismicity of the Wabash Valley seismic zone based on a temporary seismic-array experiment. *Seismological Research Letters*, *73*(5), 751–761. https://doi.org/10.1785/gssrl.73.5.751

Petersen, M. D., Shumway, A. M., Powers, P. M., Mueller, C. S., Moschetti, M. P., Frankel, A. D., et al. (2020). The 2018 update of the US national seismic hazard model: Overview of model and implications. *Earthquake Spectra*, *36*(1), 5–41. https://doi.org/10.1177/8755293019878199

Rumpfhuber, E. M., Keller, G. R., Sandvol, E., Velasco, A. A., & Wilson, D. C. (2009). Rocky mountain evolution: Tying continental dynamics of the rocky mountains and deep probe seismic experiments with receiver functions. *Journal of Geophysical Research*, *114*(B8), B08301. https://doi.org/10.1029/2008jb005726

Sbar, M. L., & Sykes, L. R. (1973). Contemporary compressive stress and seismicity in eastern North America: An example of intra-plate tectonics. *The Geological Society of America Bulletin*, *84*(6), 1861–1882. https://doi.org/10.1130/0016-7606(1973)84<1861:ccsasi>2.0.co;2

Shen, W., & Ritzwoller, M. H. (2016). Crustal and uppermost mantle structure beneath the United States. *Journal of Geophysical Research: Solid Earth*, *121*(6), 4306–4342. https://doi.org/10.1002/2016jb012887

Shen, W., Ritzwoller, M. H., & Schulte-Pelkum, V. (2013). A 3-D model of the crust and uppermost mantle beneath the Central and Western US by joint inversion of receiver functions and surface wave dispersion. *Journal of Geophysical Research: Solid Earth*, *118*(1), 262–276. https://doi.org/10.1029/2012jb009602

Stein, S., Geller, R. J., & Liu, M. (2012). Why earthquake hazard maps often fail and what to do about it. *Tectonophysics*, *562*, 1–25. https://doi.org/10.1016/j.tecto.2012.06.047

Stein, S., Stein, C. A., Elling, R., Kley, J., Keller, G. R., Wysession, M., et al. (2018). Insights from North America's failed midcontinent rift into the evolution of continental rifts and passive continental margins. *Tectonophysics*, *744*, 403–421. https://doi.org/10.1016/j.tecto.2018.07.021

Sykes, L. R. (1978). Intraplate seismicity, reactivation of preexisting zones of weakness, alkaline magmatism, and other tectonism postdating continental fragmentation. *Reviews of Geophysics*, *16*(4), 621–688. https://doi.org/10.1029/rg016i004p00621

Thybo, H., & Artemieva, I. M. (2013). Moho and magmatic underplating in continental lithosphere. *Tectonophysics*, *609*, 605–619. https://doi.org/10.1016/j.tecto.2013.05.032

Van Schmus, W. R., Bickford, M. E., & Turek, A. (1996). Proterozoic geology of the east-central midcontinent basement. *Geological Society of America Special Paper*, *308*, 7–32.

Wessel, P., & Smith, W. H. (1998). New, improved version of generic mapping tools released. *Eos, Transactions American Geophysical Union*, *79*(47), 579. https://doi.org/10.1029/98eo00426

Whitmeyer, S. J., & Karlstrom, K. E. (2007). Tectonic model for the proterozoic growth of North America. *Geosphere*, *3*(4), 220–259. https://doi.org/10.1130/ges00055.1

Williams, R. A., McCallister, N. S., & Dart, R. L. (2011). *20 cool facts about the New Madrid seismic zone-commemorating the bicentennial of the New Madrid earthquake sequence, December 1811-February 1812 [poster] (No. 134)*. US Geological Survey.

Yang, X., Pavlis, G. L., Hamburger, M. W., Marshak, S., Gilbert, H., Rupp, J., et al. (2017). Detailed crustal thickness variations beneath the Illinois Basin area: Implications for crustal evolution of the midcontinent. *Journal of Geophysical Research: Solid Earth*, *122*(8), 6323–6345. https://doi.org/10.1002/2017jb014150

Yang, X., Pavlis, G. L., Hamburger, M. W., Sherrill, E., Gilbert, H., Marshak, S., et al. (2014). Seismicity of the Ste. Genevieve seismic zone based on observations from the EarthScope OIINK flexible array. *Seismological Research Letters*, *85*(6), 1285–1294. https://doi.org/10.1785/0220140079

Zandt, G., Gilbert, H., Owens, T. J., Ducea, M., Saleeby, J., & Jones, C. H. (2004). Active foundering of a continental arc root beneath the southern Sierra Nevada in California. *Nature*, *431*(7004), 41–46. https://doi.org/10.1038/nature02847

Zhan, Y., Gregg, P. M., Chaussard, E., & Aoki, Y. (2017). Sequential assimilation of volcanic monitoring data to quantify eruption potential: Application to Kerinci volcano, Sumatra. *Frontiers of Earth Science*, *5*, 108. https://doi.org/10.3389/feart.2017.00108

Zhu, L., & Kanamori, H. (2000). Moho depth variation in southern California from teleseismic receiver functions. *Journal of Geophysical Research*, *105*(B2), 2969–2980. https://doi.org/10.1029/1999jb900322

## References From the Supporting Information

Bonvalot, S., Balmino, G., Briais, A., Kuhn, M., Peyrefitte, A., Vales, N., & Sarrailh, M. (2012). *World gravity map*. Commission for the Geological Map of the World. https://doi.org/10.14682/2012GRAVISOST